ACSNANO

www.acsnano.org

ARTICLE

Two-Dimensional 1T-Phase Transition Metal Dichalcogenides as Nanocarriers To Enhance and Stabilize Enzyme Activity for Electrochemical Pesticide Detection

Muhammad Zafir Mohamad Nasir,[†] Carmen C. Mayorga-Martinez,[†] Zdeněk Sofer,[‡] and Martin Pumera*[,†]

[†]Division of Chemistry and Biological Chemistry, School of Physical and Mathematical Sciences, Nanyang Technological University, Singapore 637371, Singapore

[‡]Department of Inorganic Chemistry, University of Chemistry and Technology Prague, Technická 5, 166 28 Prague 6, Czech Republic

Supporting Information

ABSTRACT: Single or few layers lithium-exfoliated transition metal dichalcogenides (TMDs) are found to exist predominantly in the conducting metallic 1T-polymorph, which makes it desirable for numerous applications due to its large surface area, good electrical conductivity, and enhanced electrocatalytic capabilities. We demonstrated the use of *tert*-butyllithium exfoliated TMDs (MoS_2, $MoSe_2$, WS_2, WSe_2) as a platform for the indirect electrochemical detection of an organophosphate pesticide, fenitrothion, via enzymatic inhibition pathway. All four reported materials enhanced the response of the enzymatic biosensor in comparison to the corresponding biosensor in the absence of TMDs. 1T-Phase WS_2 outperforms all other TMD materials, and we proved that it serves as an excellent transducer for enhancing electron transfer in a robust model enzyme-based inhibition assay system using cross-linking immobilization with glutaraldehyde. The reported system showed a broad fenitrothion concentration range (1−1000 nM) with an excellent linearity (r = 0.987). Moreover, the system displayed high sensitivity with low limit of detection (2.86 nM) obtained, which far exceeds the required limit set by Food and Agriculture Organisation (FAO) of the United Nations (UN). The feasibility of the proposed system in real samples was demonstrated in apple juice samples with good recoveries of 80.2% and 80.3% obtained at 10 and 1000 nM fenitrothion, respectively.

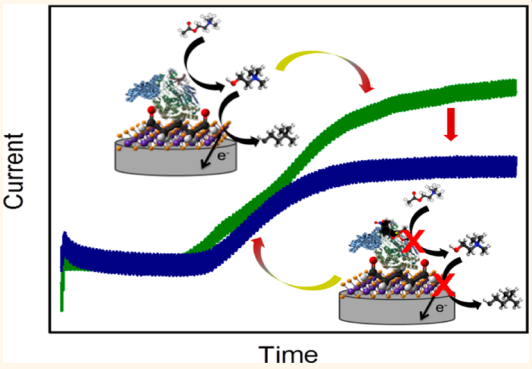

KEYWORDS: *fenitrothion, organophosphate pesticide, acetylcholinesterase, 1T-phase, transition metal dichalcogenides, tungsten disulfide, enzyme biosensor*

Transition metal dichalcogenides (TMDs) are a new class of layered materials, analogous to graphene, which have gained significant interest among scientists[1,2] due to their good physical and chemical properties.[3−8] Exfoliation of the TMDs into single or few layer sheets was discovered to enhance the chemical properties of TMDs as a result of the increased available surface area and tuning of their electronic properties.[9] This allows for potential applications in capacitors,[4,10] batteries,[4,9] vapor sensing,[11] and biosensing applications.[12−14] Different exfoliation procedures have been reported with chemical exfoliation being the most commonly practiced. Recently, it was discovered that exfoliation with *tert*-butyllithium (*t*-BuLi) produced TMD sheets with a high composition of metallic 1T-phase structures.[15] This metal-like property could be advantageous in constructing an analytical device,[11,16] which utilizes the metal-like nature of 1T-phase TMDs in enhancing sensitivity for analytical detection.

The increase in global population has generated a need to increase the global food supply, which has led to more research performed to increase crop productivity and yield. Such developments have evolved commercial farming techniques with greater emphasis placed on crop management and pest control. Organophosphorus pesticides have been developed and widely used to counter the loss of crop yield from pests' invasions. Pesticides are also commonly used for household

Received: February 26, 2017
Accepted: May 28, 2017
Published: June 6, 2017

DOI: 10.1021/acsnano.7b01364
ACS Nano 2017, 11, 5774−5784

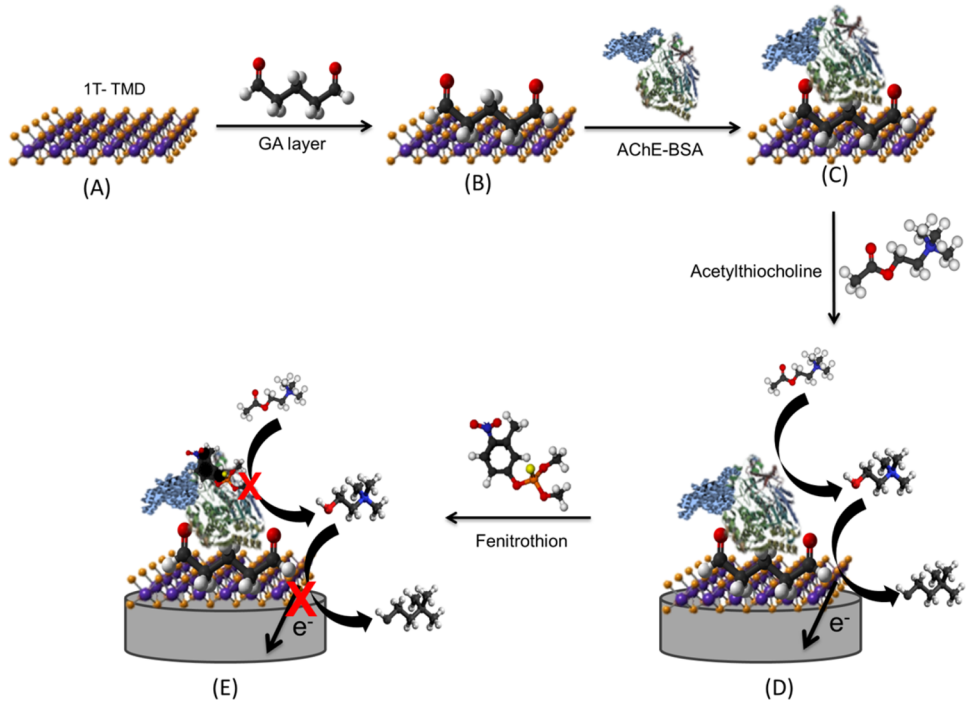

Figure 1. Illustration on the construction of the proposed pesticide biosensor: (A) loading of glassy carbon electrode with *t*-BuLi exfoliated 1T-phase TMDs, (B) conjugation with glutaraldehyde (GA) layer, (C) immobilization of acetylcholinesterase-bovine saline albumin mixture (AChE-BSA) on the modified surface, (D) the enzymatic hydrolysis of acetylthiocholine with the subsequent electrochemical oxidation of thiocholine produced, and (E) the inhibition effect of fenitrothion on AChE.

uses. Lately, there is also an increased need for detection of phosphorus compounds due to their use in chemical weapons such as sarin.[17] With such widespread and diversified use, there is the potential for excess pesticides to leech into the environment, which could lead to contamination. Numerous global and governmental agencies have invested heavily in enforcing high safety standards in food produce. Organophosphate pesticide is an example of a harmful chemical closely monitored as it can cause harmful effects to human physiology and health[18] if the residues are present in huge quantities. Fenitrothion is a commonly used organophosphate pesticide in agriculture for pest control. It binds irreversibly to the active sites of acetylcholinesterase (AChE) found on the synaptic membranes on nerve cells along the nervous system,[19] which inhibits the enzyme and renders it inactive. This prevents the breakdown of neurotransmitter acetylcholine, which leads to its accumulation in the nerve junctions thus resulting in overstimulation in the nervous system. Long-term exposure could lead to severe health problems in human population[20] and even death.[21] It is also well-absorbed from numerous routes such as ingestion, respiratory tract, and even through the skin.[22] As such, it is of utmost importance to develop an effective technique for accurate detection and quantification of pesticides in environmental and biological samples.

The development of electrochemical biosensors has mainly focused on the modification of electrodes with carbon-based materials, such as graphene[23,24] and carbon nanotubes.[25−27] These materials act as transducers in improving sensitivity and amplifying the response generated. More recently, nanoparticles[28] have been incorporated to further improve the accuracies and limits of detection. The use of other layered materials such as TMDs in enzymatic biosensors for the detection of pesticides is still unexplored and literature is lacking. TMDs would be a more favorable and attractive alternative in the fabrication of biosensors due to their lower cytotoxicity[29] and greater tunability as compared to graphene and other carbon-based materials. Besides that, the metallicity of exfoliated TMDs is expected to enhance the response signal of biosensor assay systems. TMDs have recently been used as labels in immunoassays,[16] quencher in genosensing systems,[30,31] and a platform to enhance the electrochemical signal in DNA and H_2O_2 sensing.[32,33] From our search, there have been no reports on the use of TMDs in enzymatic biosensor applications for pesticide detection. As such, we set forth to investigate the effectiveness of 1T-phase exfoliated TMDs as a platform for the detection of fenitrothion in the robust enzymatic-based inhibition assay as a model system. We adopted an acetylcholinesterase inhibition assay model as a basis of comparison to investigate the effectiveness and durability of the exfoliated TMD for such application. Henceforth, we aim to develop a biosensor based on immobilization of AChE on 1T-phase *t*-BuLi exfoliated TMD.

RESULTS AND DISCUSSION

The enzymatic biosensor was fabricated as described in the Experimental Section and schematically illustrated in Figure 1. In summary, the respective *t*-BuLi exfoliated TMD was first deposited onto a glassy carbon (GC) electrode followed by the deposition of a glutaraldehyde (GA) layer before the final immobilization of acetylcholinesterase−bovine saline albumin (AChE−BSA) mixture. Glutaraldehyde was used because it serves as a cross-linker between the protein groups in AChE and *t*-BuLi exfoliated TMD to hold the enzymes in place as well as provide structural stability to the biosensor system. AChE is the enzyme of choice due to its specificity, high turnover number, and catalytic power.[19] It is a hydrolase enzyme that catalyzes the breakdown of neurotransmitter acetylcholine to

DOI: 10.1021/acsnano.7b01364
ACS Nano 2017, 11, 5774−5784

choline and acetic acid (eq 1). Choline formed is an electroactive compound that can be oxidized and detected

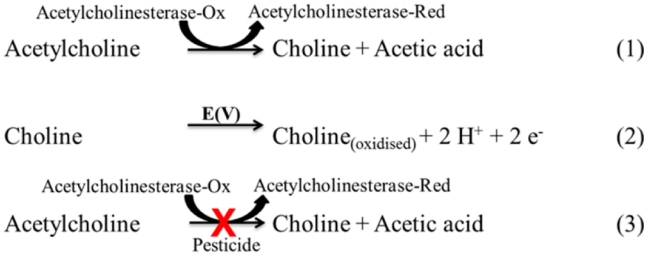

electrochemically (eq 2). The presence of oxidized choline in the solution will be detected by voltammetry and chronoamperometry. BSA serves as a blocking agent to prevent nonspecific binding onto the enzyme molecule.[34,35] It will also ensure the optimum interaction of substrate with the active site of AChE and amplify the response generated. Organophosphate pesticides are irreversible inhibitors that form strong covalent bonds between the phosphate groups of the pesticide and the hydroxyl groups within the serine residues in the active site of the enzyme. This results in the formation of a stable enzyme−pesticide complex where the enzyme gets phosphorylated and inhibited. With the binding of fenitrothion to the active site of AChE, it forms a barrier at the active site of the enzyme, which prevents the binding of acetylcholine (eq 3). Thus, the amount of acetylcholine catalyzed decreases based on the concentrations of fenitrothion present.

Characterization was first carried out to better understand the synergistic interactions, chemical composition, and morphologies of the materials. It will also affirm the metallicity of the respective *t*-BuLi exfoliated TMDs. X-ray photoelectron spectroscopy (XPS) was performed to analyze the surface elemental composition and bonding interactions involved in the respective exfoliated TMDs. Figure 2 shows high resolution spectra of deconvoluted peaks for Mo 3d and W 4f modes for the respective *tert*-butyllithium (*t*-BuLi) exfoliated TMDs. The $3d_{5/2}$ and $3d_{3/2}$ bonding modes were analyzed for molybdenum. Upon analysis of the high-resolution spectra for the molybdenum-based exfoliated TMDs, three distinct pairs of peaks were observed corresponding to the 2H and 1T polymorphs, as well as the Mo(VI) oxidized state. $MoSe_2$ showed a significant presence of 1T polymorph from the higher intensity of the respective 1T peaks with a small contribution of the semiconducting 2H polymorph (Figure 2B). However, deconvolution of the Mo 3d spectrum for *t*-BuLi exfoliated MoS_2 showed a predominance of the semiconducting 2H polymorph, as denoted by the greater intensities of the various 2H peaks (Figure 2A). The XPS results would suggest a lesser extent of exfoliation for MoS_2 in comparison to that of $MoSe_2$. This would also suggest that the *t*-BuLi exfoliated MoS_2 will be a less sensitive transducer material. Peaks present at high binding energies (greater than 230 eV) suggest the presence of oxidized products of molybdenum (Mo^{6+}), which exists in rather significant proportions. In the case of tungsten-based TMDs, the $4f_{7/2}$ and $4f_{5/2}$ bonding modes were analyzed. Three distinct pairs of peaks were also noted for tungsten-based exfoliated TMDs. In contrast, both *t*-BuLi exfoliated WS_2 and WSe_2 showed dominance of metallic 1T polymorph over the semiconducting 2H polymorph in the structures after exfoliation (Figure 2C,D). It was interesting to note that tungsten-based TMDs showed a greater proportion of 1T-phase than the molybdenum counterparts with more intense peaks observed. There is also a significant percentage of the oxidized form of tungsten (W^{6+}) as evident from the peaks present at higher binding energies (greater than 35 eV). From

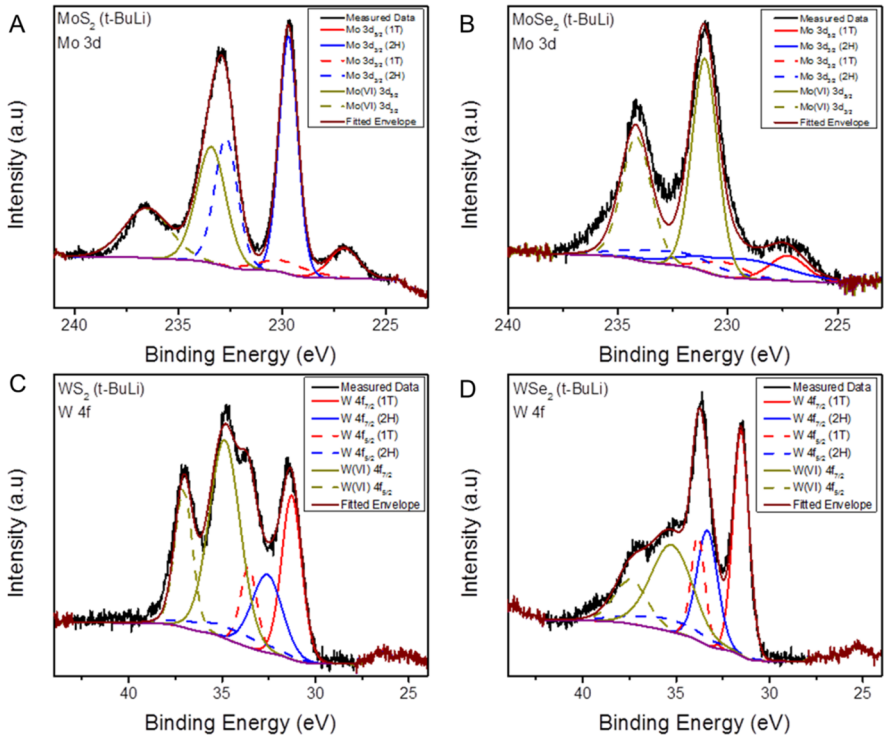

Figure 2. High-resolution X-ray photoelectron spectroscopy (XPS) spectra of Mo 3d and W 4f modes for *tert*-butyllithium (*t*-BuLi) exfoliated (A) MoS_2, (B) $MoSe_2$, (C) WS_2, and (D) WSe_2.

DOI: 10.1021/acsnano.7b01364
ACS Nano 2017, 11, 5774−5784

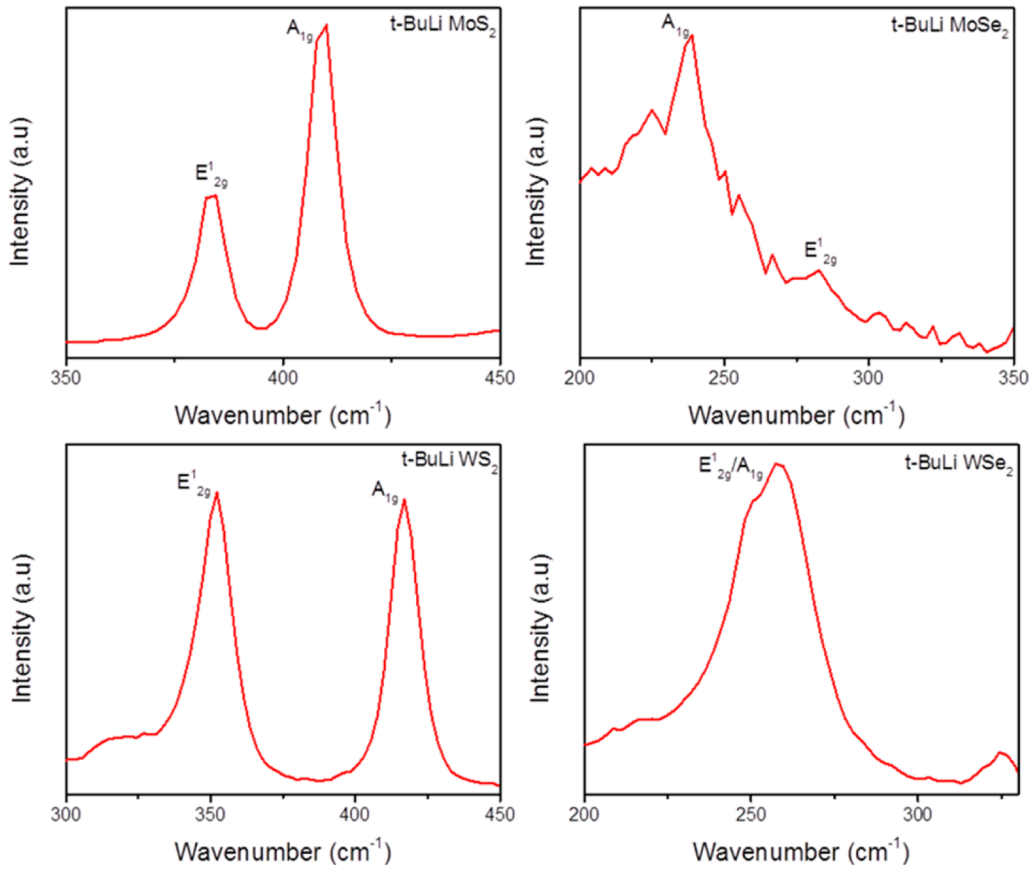

Figure 3. Raman spectra for *t*-BuLi exfoliated (A) MoS_2, (B) $MoSe_2$, (C) WS_2, and (D) WSe_2.

the XPS spectra, it was evident that the molybdenum-based TMDs have lower efficiency of conversion from 2H polymorph to 1T polymorph upon exfoliation as previously reported.[15] High-resolution XPS spectra of S 2p and Se 3d modes were also performed (see Figure S1).

Raman spectroscopy was next carried out as it is able to observe the extent of exfoliation of the respective TMDs with great sensitivity. The differences in the features of the peaks at the respective vibrational modes changes with varying layer thickness.[36] Comparison between the respective bulk[37,38] and *t*-BuLi exfoliated TMDs was carried out to observe any such deviations. The in-plane E^1_{2g} and out-of-plane A_{1g} vibrational modes were analyzed in the Raman spectra for all *t*-BuLi exfoliated TMDs as they are Raman active modes,[39] consistent with the D_{6h} point group of the respective bulk TMDs.[40] For both MoS_2 and $MoSe_2$ (Figure 3A,B), exfoliation with *t*-BuLi resulted in the broadening and softening of the E^1_{2g} and A_{1g} bands in comparison to the bulk counterparts. The A_{1g} band appears at a higher frequency than the E^1_{2g} band for $MoSe_2$, as compared to MoS_2, which correlates with previous observations.[41,42] The broadening of the A_{1g} band in $MoSe_2$ is more distinct as compared to the E^1_{2g} band, which remains almost unchanged. This correlates with previous findings where the E^1_{2g} band remains unchanged and unaffected. The broadening effect observed can been attributed to phonon confinement effect and the decrease in lattice size.[43,44] The Raman spectrum for WS_2 was next studied. A visible indication on the extent of exfoliation will be the change in $I_{A_{1g}}/I_{E^1_{2g}}$ ratio, which will increase with decreasing WS_2 thickness.[45] From Figure 3C, the intensity of E^1_{2g} band increased in comparison to that from the bulk material, which correlates to an increase in the observed $I_{A_{1g}}/I_{E^1_{2g}}$ ratio. Hence, it can be inferred that *t*-BuLi has successfully intercalated and exfoliated bulk WS_2. Lastly, for WSe_2, the E^1_{2g} and A_{1g} bands are degenerate and would result in the formation of a single peak in the bulk material. The splitting of the degenerate peaks becomes pronounced with the exfoliation of the bulk material.[46] Figure 3D shows the presence of two small peaks closely located at about 250 and 253 cm^{-1}, which overlap as a single broad peak. It can thus be postulated from the splitting of the degenerate peaks that WSe_2 was exfoliated by *t*-BuLi. From the Raman spectroscopy and XPS studies, it suggests that the lithium exfoliation of tungsten-based TMDs appears to be more effective and efficient in comparison to their molybdenum counterparts. From the respective characterization studies conducted, it can be concluded that the *t*-BuLi exfoliated TMDs exhibit metal-like characteristics and exist predominantly in the 1T polymorph, which will aid in the response amplification for the model enzymatic inhibition biosensor assay.

It is of utmost interest to evaluate the performances of the different *t*-BuLi exfoliated 1T-TMDs (MoS_2, $MoSe_2$, WS_2, WSe_2) to monitor any differences in sensitivity and response based on their different inherent properties. We next set forth to investigate the feasibility of the proposed biosensor system for the detection of fenitrothion. Chronoamperometric measurements were carried out to analyze the response of the pesticide biosensing system fabricated using the different *t*-BuLi exfoliated TMDs through successive injection of acetylthiocholine. All four materials showed enhanced biosensor performance as compared to biosensor without TMDs

DOI: 10.1021/acsnano.7b01364
ACS Nano 2017, 11, 5774−5784

(green line of Figure 4). $MoSe_2$ and WSe_2 showed similar responses, which were lower than MoS_2 and WS_2. It was

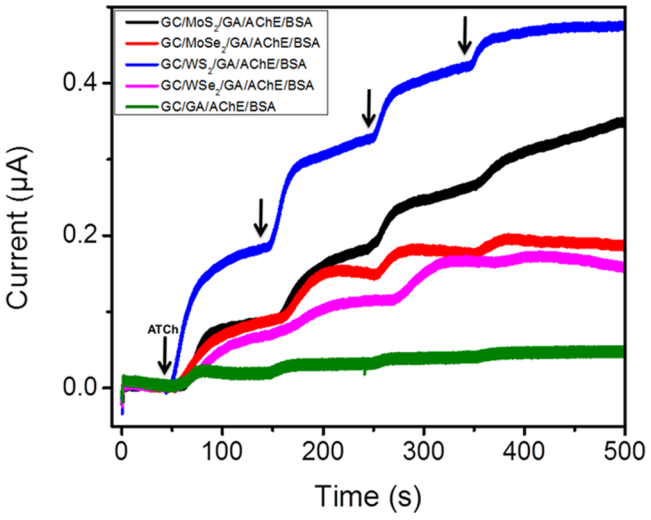

Figure 4. Chronoamperometric measurements with successive injection of ATCh on different *t*-BuLi exfoliated TMD modified biosensor in 0.01 M PBS. Arrows indicate the point of injection of ATCh (concentration of ATCh = 500 μM).

interesting to note that MoS_2 outperformed both $MoSe_2$ and WSe_2 despite being predominantly in the 2H polymorph. A possible reason for the rather sensitive response could be the successful exfoliation of MoS_2 into few layered sheets. 1T-WSe_2 displayed the lowest sensitivity, which is contrary to the results from characterization studies. This anomaly could suggest the smaller extent of exfoliation of WSe_2 and its existence in multiple layers thus providing a lower surface area. As such, the metal-like properties are compromised and the sensitivity is reduced. The greater sensitivity of WS_2 in comparison to WSe_2 would also suggest successful exfoliation of the bulk material as evident from the greater separation of the E^1_{2g} and A_{1g} vibrational modes for WS_2 (Figure 3C). It was also interesting to note that sulfur-based dichalcogenides performed better than their selenide-based counterparts. Moreover, 1T-phase WS_2 is demonstrated to provide also increased density of catalytic active sites that for the 1T-phase materials are on both the basal plane and edges.[47−50] All of these capabilities of 1T-phase facilitate the electrochemical oxidation of thiocholine in the proposed biosensor (Figure 1D and eq 2). From the studies performed, it can be deduced that 1T-WS_2 is the most suitable TMD for further electrochemical biosensor fabrication.

Initial studies with 1T-WS_2 modified biosensor using cyclic voltammetry showed a small anodic peak at 0.1 V in the presence of acetylthiocholine iodide (Figure S2). However, a significantly enhanced current intensity was observed in the CV of the biosensor in the presence of acetylthiocholine iodide (red line) in comparison with the biosensor without analyte (black line). From the voltammogram obtained, it was decided that a potential of 0.1 V would be used as the applied potential for further chronoamperometric studies. This potential was chosen as it is relatively low and away from the anodic potential of possible interference signals such as polyphenols, vitamins, and others (see Figure S3). Higher and lower potentials were also tested, and the best response was observed with 0.1 V.

The metallic nature and increased density of catalytic active sites of 1T-WS_2 enhanced the current response signal from the oxidation of thiocholine produced from the enzymatic catalysis of acetylthiocholine, and thus the oxidation potential gets shifted to a lower anodic potential as shown in Figure S2. A similar observation on the shift in oxidation potential of thiocholine in pesticide based on nanomaterials was previously reported for carbon nanotubes,[51] composites of polyaniline/carbon nanotubes,[52,53] and Au nanoparticles dispersed in carbon nanotubes.[54]

Having ascertained that the enzymatic biosensor assay system is feasible, we proceed to study any effects of intereferences on the proposed system. Chronoamperometric analysis was performed at 0.1 V with Fe^{2+}, Cu^{2+}, ascorbic acid, and phenol (Figure S3). The compounds were chosen as they are commonly found in most variants of fruits and the respective concentrations reflect closely their physiological concentrations.[55] From Figure S3, it was determined that the mentioned compounds do not interfere significantly with the oxidation signal of acetylthiocholine (current change <7%), which validates the use of low working potential. Utilizing this information, we next set forth to carry out chronoamperometry for subsequent procedures at 0.1 V.

The extent of exfoliation of the 1T-WS_2 was further analyzed with TEM, selected area electron diffraction (SAED), and HR-

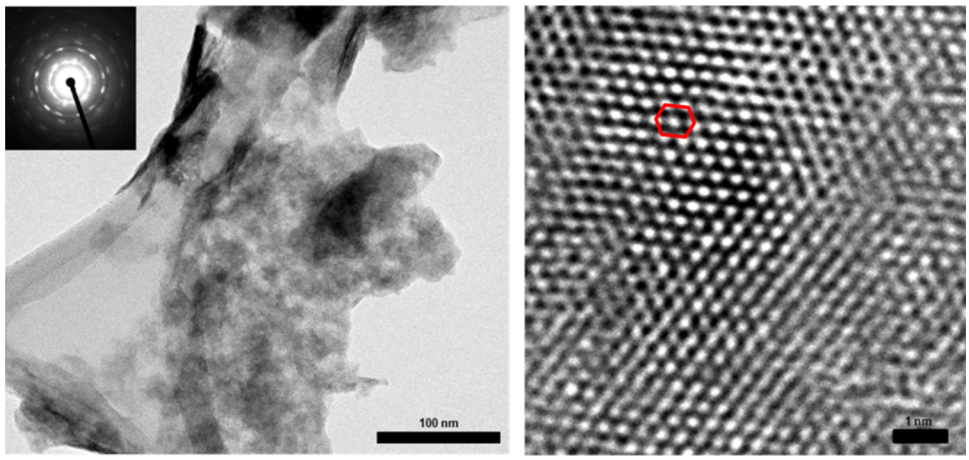

Figure 5. Transmission electron microscopy (TEM) image with selected area electron diffraction (SAED) pattern (insert) of WS_2. High resolution TEM (HR-TEM) images show dominant presence of 1T-phase (red hexagon). Scale as indicated in the images, respectively.

DOI: 10.1021/acsnano.7b01364
ACS Nano 2017, 11, 5774−5784

TEM (Figure 5). From the TEM image, exfoliation of the materials is evident with the presence of few layer sheets of about 1 μm observed. SEM image also shows similar observations with few layers observed for 1T-WS_2 (Figure S4A). SAED pattern showed hexagonal symmetry of WS_2. HR-TEM image further validates the 1T-phase of WS_2 from the hexagonal arrangement of atoms, which corresponds to 1T-phase arrangement. These findings validate the results obtained from XPS and Raman spectroscopy in validating the 1T polymorph and extent of exfoliation of WS_2 used in the model enzymatic biosensor.

Chronoamperometry was performed, and the chronoamperometric responses were observed with successive injection of acetylthiocholine to the different modified layers. From Figure 6, there was no visible current response for measurements carried out on bare glassy carbon. Modification of the glassy carbon electrode with WS_2 resulted in a small increase in the current response upon injection of acetylthiocholine. The signal generated could be from the oxidation of small quantities of iodide counterions present with acetylthiocholine used[56,57] (Figure S5 and S6). GC/WS_2/GA and GC/WS_2/BSA showed low chronoamperometric responses, which validates the absence of the catalytic activity of enzyme. The importance of enzyme AChE is evident with an enhanced response obtained after injection of acetylthiocholine. The significant increase in response upon the immobilization of AChE can be attributed to the high turnover number and strong catalytic power[19,58] of the enzyme, which was found to catalyze about 10^4 molecules per second.[59] With more acetylthiocholine being catalyzed, the amount of thiocholine present greatly increased, and thus more thiocholine gets oxidized in return. An enhanced response was further obtained upon the introduction of BSA to AChE. This could correlate to more electroactive thiocholine produced and lesser acetylthiocholine lost from nonspecific binding of the AChE. The combined effect of the metal-like property and enhanced catalytic activity of *t*-BuLi exfoliated 1T-WS_2 enables more efficient electro-oxidation of thiocholine and greater amount of enzymes to be immobilized to get better sensitivity of the model enzymatic inhibition biosensor. As such, the exfoliated material aids in improving the sensitivity and response signal of this system. The chronoamperometric measurements carried out validates the importance of the different layers in the proposed biosensor and their successful immobilization in the preparation steps. It further proves the robustness and stability of the biosensor system that was used as a model assay to evaluate the electrocatalytic effect of different TMDs exfoliated by t-butyllithium.

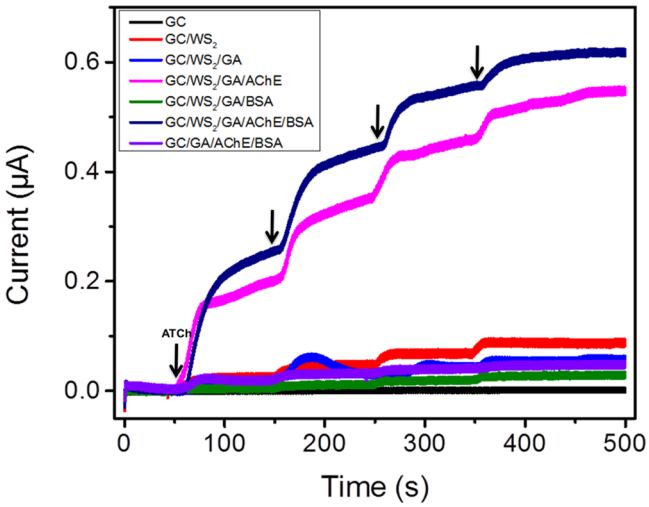

Figure 6. Chronoamperometric measurements with successive injection of ATCh on each modified layer of the proposed biosensor system in 0.01 M PBS. Arrows indicate the point of injection of ATCh (Concentration of ATCh = 500 μM).

The inhibition effect of fenitrothion on the enzymatic biosensor system was next studied. Initial cyclic voltammetry (CV) scans on the modified electrodes were performed. It was noted that the anodic peak diminishes in the presence of fenitrothion (Figure S7) with a corresponding decrease in current intensity of the CV after inhibition with fenitrothion. Chronoamperometric studies were subsequently performed to analyze the inhibition effect of fenitrothion with the proposed biosensor system (Figure 7). In the absence of fenitrothion, injection of acetylthiocholine (500 μM) saw a sharp increase in current signal which gradually becomes steady. The current response obtained after inhibition with fenitrothion showed a decrease in current response by about 0.05 μA. The drop in current signal obtained is indicative of less thiocholine being oxidized, which corroborates a decrease in the amount of acetylthiocholine catalyzed by AChE. Fenitrothion was successful in binding irreversibly to the active site of AChE, which hindered the catalysis of acetylthiocholine and suppressed the signal obtained. From these initial observations, it can be concluded that the biosensor is responsive to the presence of fenitrothion as evident from the decrease in response current.

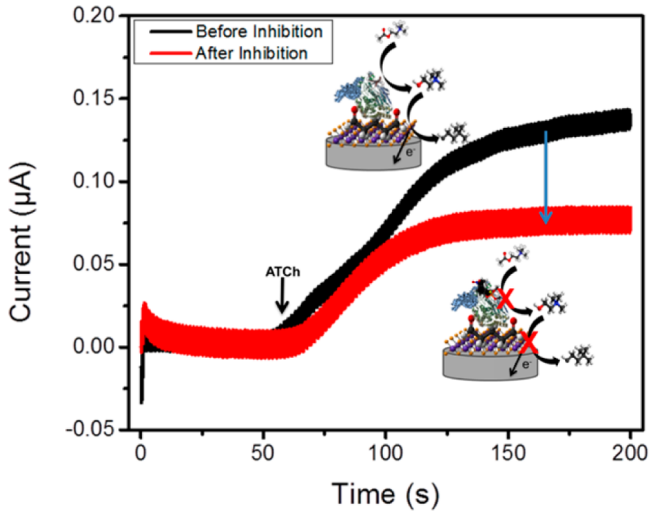

Figure 7. Chronoamperometric measurements showing the inhibition effect of fenitrothion on 1T-WS_2 modified biosensor system in 0.01 M PBS. Black arrow indicates the point of injection of ATCh, and blue arrow indicates the drop in current response observed after inhibition with fenitrothion (concentration of ATCh = 500 μM).

We next set forth to study various experimental parameters to optimize the performance of the biosensor. As mentioned previously, AChE gets phosphorylated when fenitrothion forms a covalent bond with the hydroxyl group of the serine residues in the active site thus inhibiting the enzyme. The response generated from the electrochemical oxidation of thiocholine thus decreases with increasing exposure to fenitrothion. Using

DOI: 10.1021/acsnano.7b01364
ACS Nano 2017, 11, 5774−5784

this concept, the degree of inhibition can be measured based on the change in thiocholine signal response before and after fenitrothion inhibiton. The inhibition percentage (I%) was calculated as a means to evaluate the extent of inhibition before (I_b) and after incubating (I_a) with fenitrothion (eq 4) to analyze the inhibition activity of fenitrothion on AChE. A higher I% would be favorable as it indicates greater inhibition of enzymes, which correlates to better performance of the biosensor.

$$I(\%) = \frac{[(I_b - I_a)]}{I_b} \times 100 \quad (4)$$

The first parameter of interest is acetylthiocholine concentration. Acetylthiocholine serves as the substrate for enzymatic catalysis. A substrate concentration that is higher than the turnover number of the enzyme could slow down the response time due to saturation at the active site of the enzymes. However, substrate concentrations that are too low could generate weak or negative response. It is thus important to choose a suitable concentration to ensure optimum working capacity of the enzymes. Three different acetylthiocholine concentrations (50, 100, and 250 μM) were studied. Figure 8A shows I% for the different acetylthiocholine concentrations, which increases with increasing concentration. Acetylthiocholine concentration of 50 μM produced negative I%, which suggests insufficient substrate present to interact with the enzymes. Acetylthiocholine concentration of 250 μM showed greater I% as compared to a concentration of 100 μM and was thus selected as the working concentration for the experiment.

We next set forth to optimize the amount of 1T-WS_2 to be deposited onto glassy carbon electrode. 1T-WS_2 serves as the transducer for electron transfer, and it is important to ensure optimum loading of the material onto the electrode surface. Three different WS_2 concentrations (1, 5, and 10 mg mL^{-1}) were studied. From Figure 8B, the optimum concentration to be deposited is 1 mg mL^{-1}, and it was the only concentration with positive I%. Higher concentrations of WS_2 (5 and 10 mg mL^{-1}) gave negative I%, which might suggest saturation or passivation of the electrode surface. Besides that, the higher concentrations might have caused an excess of WS_2 to be deposited, which could have created a barrier and hindered electron transfer. As such, WS_2 concentration of 1 mg mL^{-1} was chosen as the optimum concentration to be loaded onto the electrode surface.

The last variable optimized is pesticide inhibition time. A lower response will be obtained when the pesticide binds irreversibly to the active site of the enzyme. It is thus important to optimize this variable to allow sufficient time for fenitrothion to bind to the active site of the enzymes to optimize I% results. However, the time domain should also not be too long for on-site analysis. Three different inhibition times (5, 15, and 30 min) were chosen. From Figure 8C, inhibition times of 5 and 15 min showed similar I% results. It was also interesting to observe that the longest inhibition time of 30 min showed the lowest I% result. The long inhibition time might have saturated the enzyme as it reaches its turnover rate. The enzymes could also have detached from the modified surface during the long time duration. Five minute inhibition time was chosen due to its better reproducibility with the smallest error bar obtained. The shorter time duration was also taken into consideration as an important criteria to be an efficient on-site, point-of-care analytical device.

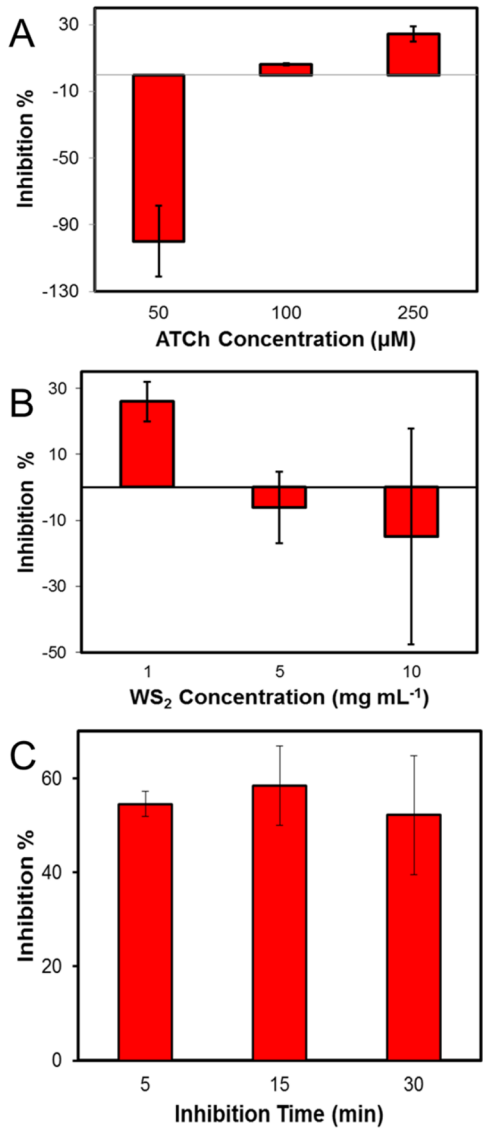

Figure 8. Optimization of (A) ATCh concentration, (B) WS_2 concentration, and (C) fenitrothion inhibition time.

The analytical response of the model biosensor system with the optimized parameters was then examined using chronoamperometry with injection of acetylthiocholine into stirred 0.01 M PBS. Increasing the fenitrothion concentration is predicted to generate greater inhibition of AChE, which will correlate to decreased catalytic activity (see Figure 8) and hence generate a greater I% value. Figure 9A shows the linear plot for fenitrothion concentrations between 1 and 1000 nM for the proposed biosensor system with r = 0.987. The limit of detection (LOD) was calculated by multiplying the quotient of the standard deviation of the chronoamperometric current of the lowest concentration of pesticide and gradient for the calibration graph by 3, and limit of quantification (LOQ) was obtained by multiplying the same quotient described previously by 10.[60−64] The system has a low LOD of 2.86 nM and LOQ of 9.54 nM. A new modified electrode has to be used for each experiment after exposure to fenitrothion due to the irreversible binding of the pesticide to the enzymes. The RSD is the average of 4 different concentrations where each concentration was measured 4 times. The error bars obtained are hence a result of same day repeatability of measurements having relative

DOI: 10.1021/acsnano.7b01364
ACS Nano 2017, 11, 5774−5784

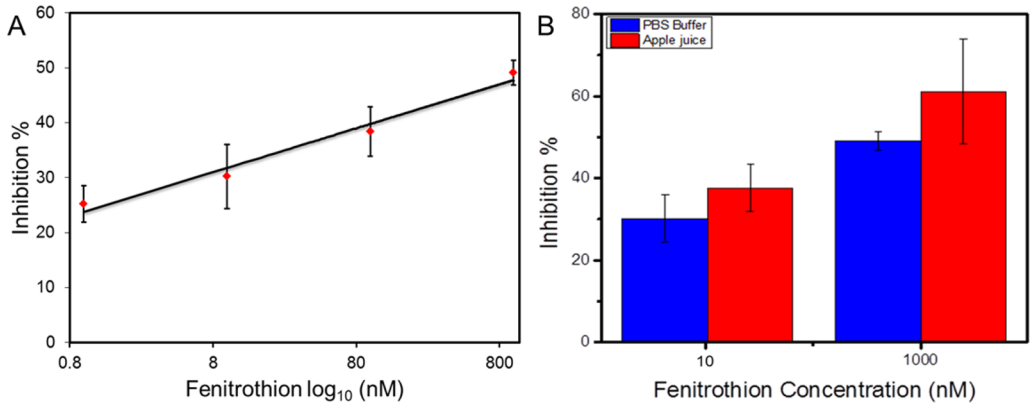

Figure 9. (A) Calibration plot showing the inhibition of biosensor vs fenitrothion concentration. (B) Recoveries with fresh apple juice for pesticide concentrations of 10 and 1000 nM.

standard deviation (RSD) of ~10%. When applying the one-way ANOVA statistical analysis with a confidence interval of 0.99, the mean values for the inhibition percentages were different with p = 0.00019. Moreover, the good linearity and analytical performance of the biosensor system makes it promising for potential applications.

Recovery experiments were then carried out to demonstrate the working capabilities of the proposed biosensor with real samples where interfering species were present. Recovery percentages were calculated as shown in eq 5. Recovery percentages of 80.2% and 80.3% were obtained at fenitrothion concentrations of 10 and 1000 μM, respectively, in fresh apple juice (Figure 9B). The results obtained suggest that the proposed biosensor system is feasible and responsive for detecting low concentrations of fenitrothion in real samples. The system also showed good reproducibility and analytical performance in detecting fenitrothion with apple juice. The model biosensor system, where t-BuLi exfoliated 1T-WS_2 was used as an active electrocatalytic platform with enhanced analytical performance, serves as a promising platform that can be extended toward the development of future TMD-based enzymatic biosensors for environmental and biomedical applications.

$$R(\%) = \left(\frac{[\text{fenitrothion}]_{\text{buffer}}}{[\text{fenitrothion}]_{\text{real-sample}}} \right) \times 100 \quad (5)$$

Moreover, the use of 1T-WS_2 has proven to outperform most carbon-based materials and provide a more sensitive alternative compared to previous works reported. Our proposed biosensor system exhibited excellent analytical performance with respect to detection limits and range in comparison to other works previously reported for fenitrothion detection (see Table S1). The analytical performance with t-BuLi exfoliated 1T-WS_2 is also comparable to the use of dispersed graphene oxide by Liu et al.[65] with similar detection range and magnitude in the limit of detection (LOD) observed. One advantage of our proposed system also is its selectivity brought about by the immobilization of AChE and low working potential (0.1 V) used. The high selectivity of AChE toward binding with organophosphate pesticides makes it attractive as a detection method for our target analytes. The use of low potential also reduces interference signals from other analytes present in real sample analysis. Besides that, the time taken for fenitrothion detection is rather short (5 min) with great reproducibility and linearity. The LOD obtained is 2.86 nM, which corresponds to 0.743 ppb. This value obtained is significantly lower than the maximum allowed quantity set by various environmental agencies such as Food and Agriculture Organisation (FAO) of the United Nations (10 ppm)[66] and Agri-Food and Veterinary (AVA) of Singapore (2 ppm).[67]

CONCLUSION

A biosensor based on a robust enzymatic-based inhibition assay was used as a model system, where AChE and t-BuLi exfoliated 1T-phase WS_2 was immobilized onto a glassy carbon electrode. This system has been developed for the effective detection of organophosphate pesticide fenitrothion. Besides that, it was demonstrated that the t-BuLi exfoliated metallic 1T-phase WS_2 shows the best performance among the other group 6 TMDs exfoliated using the same method, such as MoS_2, $MoSe_2$, and WSe_2. 1T-Phase WS_2 serves as a conductive platform transducer with increased density of catalytic sites for the efficient electrochemical oxidation of thiocholine, which enhances the amperometric response. The proposed biosensor shows good linearity with a low limit of detection (2.86 nM). Good recovery percentages are also obtained in real sample analysis with apple juice. With these findings, it also shows conceptually the possible application of TMDs in the area of biosensors and varied possibilities for the development of future TMD-based biosensors for on-site, point-of-care environmental and biological sample analysis.

EXPERIMENTAL SECTION

Materials and Apparatus. Molybdenum disulfide, molybdenum diselenide, tungsten disulfide and tungsten diselenide were obtained from Alfa Aesar (Germany). Potassium chloride, potassium hexacyanoferrate(II) trihydrate, potassium hexacyanoferrate(III), bovine serum albumin (BSA), acetylthiocholine iodide (ATChI), acetylcholinesterase (AChE) from electric eel, glutaraldehyde (GA, 50%), fenitrothion, ascorbic acid, phenol, and phosphate buffer saline (PBS) in tablets were purchased from Sigma-Aldrich (Singapore). High quality water, purified in a Milli-Q system (Millipore, MA, USA) with a resistivity of 18 MΩ cm was used. Biosan TS-100 (Latvia) thermoshaker was used to stir the samples during the inhibition process at a temperature of 37 °C with shaking at 400 rpm.

Electrochemical Measurements. Electrochemical measurements were conducted using a μAutolab Type III electrochemical analyzer (Eco Chemie, The Netherlands) controlled by NOVA 1.9 software (Eco Chemie) at room temperature (25 °C) by using a three-electrode configuration. Platinum (Pt), Ag/AgCl, and GC electrodes (diameters of 3 mm) were obtained from CH Instruments (Texas, USA).

DOI: 10.1021/acsnano.7b01364
ACS Nano 2017, 11, 5774–5784

Cyclic voltammetry (CV) experiment was performed at a scan rate of 100 mV s^{-1}. All chronoamperometry measurements were recorded at 10 ms intervals in 0.01 M PBS. A magnetic stirrer was used to assist convection.

Characterization. X-ray photoelectron spectroscopy (XPS) was carried out with a Phoibos 100 spectrometer with a monochromatic Mg X-ray source (SPECS, Germany) at 1254 eV. Transmission electron microscopy (TEM) and high resolution transmission electron microscopy (HR-TEM) was carried out with EFTEM JEOL 2200 FS microscope (JEOL, Japan) with acceleration voltage of 200 keV. Raman spectroscopy was carried out using confocal micro-Raman LabRam HR instrument (HORIBA Scientific) in backscattering geometry with CCD detector, 514.5 nm argon excitation laser, and a 100× objective lens mounted to an Olympus optical microscope. The spectra range used was from 100 to 1000 cm^{-1}. Calibration was carried out before measurements were taken using an internal silicon reference at 520 cm^{-1} with peak position resolution of less than 1 cm^{-1}. Scanning electron microscopy (SEM) was performed with JEOL 7600F-SEM (JEOL, Japan). SEM was performed on a silicon wafer operating at 2 kV.

Preparation of Exfoliated Transition Metal Dichalcogenides. Three grams of respective TMD bulk powder was suspended in 20 mL of 1.7 M *tert*-butyllithium (*t*-BuLi). Subsequently, it was stirred for 72 h at 25 °C under argon atmosphere to intercalate with Li. The intercalated material was separated by suction filtration under argon atmosphere and washed thoroughly with hexane (dried over sodium). The separated Li-intercalated material was placed in water (100 mL) before repeated centrifugation (18 000*g*) was carried out. The exfoliated material was dried in a vacuum oven at 50 °C for 48 h before use. It was later dispersed in water and ultrasonicated for 60 min to obtain a well-dispersed suspension.

Preparation of Biosensor System. AChE (1 mg in 50 μL) and 5% BSA were prepared in 0.01 M PBS. Three microliters of the suspension of *t*-BuLi exfoliated TMD of desired concentration was drop-coated on the glassy carbon (GC) electrode surface and left to dry at room temperature. Glutaraldehyde (GA), 0.25%, was prepared in ultrapure water, and 5 μL of the solution was coated onto the GC/TMD surface. Two microliters of AChE in 5% BSA (1:1) was next coated onto the modified surface. The electrodes were oven-dried at 35 °C between steps for 30 min.

Real Sample Preparation. Fresh apples were bought from a local supermarket and blended with 0.01 M PBS. The blend was filtered several times to remove any insoluble and larger particles, which may affect the measurements. The fresh juice was obtained as filtrate for further real sample analysis.

ASSOCIATED CONTENT

Supporting Information

The Supporting Information is available free of charge on the ACS Publications website at DOI: 10.1021/acsnano.7b01364.

High-resolution X-ray photoelectron spectroscopy of the chalcogens, scanning electron microscopy of WS_2, cyclic voltammograms illustrating the effect of 1T-WS_2 on the model biosensor inhibition assay, acetylthiocholine iodide on the biosensor system, influence of iodide ions and inhibition effect of fenitrothion, chronoamperometric measurements of variable fenitrothion concentrations before and after inhibition, illustration of the influence of interference analytes on the biosensor system, and table of different analytical systems for fenitrothion detection (PDF)

AUTHOR INFORMATION

Corresponding Author

*pumera.research@gmail.com.

ORCID

Martin Pumera: 0000-0001-5846-2951

Notes

The authors declare no competing financial interest.

ACKNOWLEDGMENTS

M.P. acknowledges support from Tier 2 (MOE2013-T2-1-056; ARC 35/13) from Singapore Ministry of Education. Z.S. was supported by Czech Science Foundation (GACR No. 16-05167S). This work was created with the financial support of the Neuron Foundation for science support.

REFERENCES

(1) Chhowalla, M.; Shin, H. S.; Eda, G.; Li, L.-J.; Loh, K. P.; Zhang, H. The Chemistry of Two-Dimensional Layered Transition Metal Dichalcogenide Nanosheets. *Nat. Chem.* **2013**, *5*, 263−275.

(2) Zeng, H.; Dai, J.; Yao, W.; Xiao, D.; Cui, X. Valley Polarization in MoS_2 Monolayers by Optical Pumping. *Nat. Nanotechnol.* **2012**, *7*, 490−493.

(3) Mak, K. F.; He, K.; Shan, J.; Heinz, T. F. Control of Valley Polarization in Monolayer MoS_2 by Optical Helicity. *Nat. Nanotechnol.* **2012**, *7*, 494−498.

(4) Pumera, M.; Sofer, Z.; Ambrosi, A. Layered Transition Metal Dichalcogenides for Electrochemical Energy Generation and Storage. *J. Mater. Chem. A* **2014**, *2*, 8981−8987.

(5) Wang, Q. H.; Kalantar-Zadeh, K.; Kis, A.; Coleman, J. N.; Strano, M. S. Electronics and Optoelectronics of Two-Dimensional Transition Metal Dichalcogenides. *Nat. Nanotechnol.* **2012**, *7*, 699−712.

(6) He, Z.; Que, W. Molybdenum Disulfide Nanomaterials: Structures, Properties, Synthesis and Recent Progress on Hydrogen Evolution Reaction. *Appl. Mater. Today* **2016**, *3*, 23−56.

(7) Reale, F.; Sharda, K.; Mattevi, C. From Bulk Crystals to Atomically Thin Layers of Group VI-Transition Metal Dichalcogenides Vapor Phase Synthesis. *Appl. Mater. Today* **2016**, *3*, 11−22.

(8) Li, S.; Wang, S.; Tang, D.-M.; Zhao, W.; Xu, H.; Chu, L.; Bando, Y.; Golberg, D.; Eda, G. Halide-Assisted Atmospheric Pressure Growth of Large WSe_2 and WS_2 Monolayer Crystals. *Appl. Mater. Today* **2015**, *1*, 60−66.

(9) Chia, X.; Eng, A. Y. S.; Ambrosi, A.; Tan, S. M.; Pumera, M. Electrochemistry of Nanostructured Layered Transition-Metal Dichalcogenides. *Chem. Rev.* **2015**, *115*, 11941−11966.

(10) Wang, H.; Feng, H.; Li, J. Graphene and Graphene-Like Layered Transition Metal Dichalcogenides in Energy Conversion and Storage. *Small* **2014**, *10*, 2165−2181.

(11) Mayorga-Martinez, C. C.; Ambrosi, A.; Eng, A. Y. S.; Sofer, Z.; Pumera, M. Metallic 1T-WS_2 for Selective Impedimetric Vapor Sensing. *Adv. Funct. Mater.* **2015**, *25*, 5611−5616.

(12) Huang, K.-J.; Wang, L.; Liu, Y.-J.; Gan, T.; Liu, Y.-M.; Wang, L.-L.; Fan, Y. Synthesis and Electrochemical Performances of Layered Tungsten Sulfide-Graphene Nanocomposite as a Sensing Platform for Catechol, Resorcinol and Hydroquinone. *Electrochim. Acta* **2013**, *107*, 379−387.

(13) Pumera, M.; Loo, A. H. Layered Transition-Metal Dichalcogenides (MoS_2 and WS_2) for Sensing and Biosensing. *TrAC, Trends Anal. Chem.* **2014**, *61*, 49−53.

(14) Su, S.; Sun, H.; Cao, W.; Chao, J.; Peng, H.; Zuo, X.; Yuwen, L.; Fan, C.; Wang, L. Dual-Target Electrochemical Biosensing Based on DNA Structural Switching on Gold Nanoparticle-Decorated MoS_2 Nanosheets. *ACS Appl. Mater. Interfaces* **2016**, *8*, 6826−6833.

(15) Ambrosi, A.; Sofer, Z.; Pumera, M. 2H → 1T Phase Transition and Hydrogen Evolution Activity of MoS_2, $MoSe_2$, WS_2 and WSe_2 Strongly Depends on the MX_2 Composition. *Chem. Commun.* **2015**, *51*, 8450−8453.

(16) Mayorga-Martinez, C. C.; Khezri, B.; Eng, A. Y. S.; Sofer, Z.; Ulbrich, P.; Pumera, M. Bipolar Electrochemical Synthesis of WS_2 Nanoparticles and Their Application in Magneto-Immunosandwich Assay. *Adv. Funct. Mater.* **2016**, *26*, 4094−4098.

DOI: 10.1021/acsnano.7b01364
ACS Nano 2017, 11, 5774−5784

(17) Szinicz, L. History of Chemical and Biological Warfare Agents. *Toxicology* **2005**, *214*, 167−181.
(18) Namba, T.; Nolte, C. T.; Jackrel, J.; Grob, D. Poisoning Due to Organophosphate Insecticides. Acute and Chronic Manifestations. *Am. J. Med.* **1971**, *50*, 475−492.
(19) Quinn, D. M. Acetylcholinesterase: Enzyme Structure, Reaction Dynamics, and Virtual Transition States. *Chem. Rev.* **1987**, *87*, 955−979.
(20) Ecobichon, D. J.; Ozere, R. L.; Reid, E.; Crocker, J. F. S. Acute Fenitrothion Poisoning. *Can. Med. Assoc. J.* **1977**, *116*, 377−379.
(21) Organophosphorous Insecticides: A General Introduction, World Health Organization (WHO), Genèva, 1986.
(22) Colovic, M. B.; Krstic, D. K.; Lazarevic-Pasti, T. D.; Bondzic, A. M.; Vasic, V. M. Acetylcholinesterase Inhibitors: Pharmacology and Toxicology. *Curr. Neuropharmacol.* **2013**, *11*, 315−335.
(23) Pumera, M. Graphene in Biosensing. *Mater. Today* **2011**, *14*, 308−315.
(24) Wu, S.; Lan, X.; Cui, L.; Zhang, L.; Tao, S.; Wang, H.; Han, M.; Liu, Z.; Meng, C. Application of Graphene for Preconcentration and Highly Sensitive Stripping Voltammetric Analysis of Organophosphate Pesticide. *Anal. Chim. Acta* **2011**, *699*, 170−176.
(25) Lin, Y.; Lu, F.; Wang, J. Disposable Carbon Nanotube Modified Screen-Printed Biosensor for Amperometric Detection of Organophosphorus Pesticides and Nerve Agents. *Electroanalysis* **2004**, *16*, 145−149.
(26) Kesik, M.; Kanik, F. E.; Turan, J.; Kolb, M.; Timur, S.; Bahadir, M.; Toppare, L. An Acetylcholinesterase Biosensor Based on a Conducting Polymer Using Multiwalled Carbon Nanotubes for Amperometric Detection of Organophosphorus Pesticides. *Sens. Actuators, B* **2014**, *205*, 39−49.
(27) Joshi, K. A.; Tang, J.; Haddon, R.; Wang, J.; Chen, W.; Mulchandani, A. A Disposable Biosensor for Organophosphorus Nerve Agents Based on Carbon Nanotubes Modified Thick Film Strip Electrode. *Electroanalysis* **2005**, *17*, 54−58.
(28) Wang, Y.; Zhang, S.; Du, D.; Shao, Y.; Li, Z.; Wang, J.; Engelhard, M. H.; Li, J.; Lin, Y. Self Assembly of Acetylcholinesterase on a Gold Nanoparticles−Graphene Nanosheet Hybrid for Organophosphate Pesticide Detection Using Polyelectrolyte as a Linker. *J. Mater. Chem.* **2011**, *21*, 5319−5325.
(29) Teo, W. Z.; Chng, E. L. K.; Sofer, Z.; Pumera, M. Cytotoxicity of Exfoliated Transition-Metal Dichalcogenides (MoS_2, WS_2, and WSe_2) Is Lower Than That of Graphene and Its Analogues. *Chem. - Eur. J.* **2014**, *20*, 9627−9632.
(30) Xi, Q.; Zhou, D.-M.; Kan, Y.-Y.; Ge, J.; Wu, Z.-K.; Yu, R.-Q.; Jiang, J.-H. Highly Sensitive and Selective Strategy for MicroRNA Detection Based on WS_2 Nanosheet Mediated Fluorescence Quenching and Duplex-Specific Nuclease Signal Amplification. *Anal. Chem.* **2014**, *86*, 1361−1365.
(31) Singh, V. V.; Kaufmann, K.; de Avila, B. E.-F.; Karshalev, E.; Wang, J. Molybdenum Disulfide-Based Tubular Microengines: Toward Biomedical Applications. *Adv. Funct. Mater.* **2016**, *26*, 6270−6278.
(32) Toh, R. J.; Mayorga-Martinez, C. C.; Sofer, Z.; Pumera, M. 1T-Phase WS2 Protein-Based Biosensor. *Adv. Funct. Mater.* **2017**, *27*, 1604923.
(33) Huang, K.-J.; Liu, Y.-J.; Wang, H.-B.; Gan, T.; Liu, Y.-M.; Wang, L.-L. Signal Amplification for Electrochemical DNA Biosensor Based on Two-Dimensional Graphene Analogue Tungsten Sulfide−Graphene Composites and Gold Nanoparticles. *Sens. Actuators, B* **2014**, *191*, 828−836.
(34) Gan, S. D.; Patel, K. R. Enzyme Immunoassay and Enzyme-Linked Immunosorbent Assay. *J. Invest. Dermatol.* **2013**, *133*, 1−3.
(35) Lee, J.; Park, I.-S.; Kim, H.; Woo, J.-S.; Choi, B.-S.; Min, D.-H. BSA as Additive: A Simple Strategy for Practical Applications of PNA in Bioanalysis. *Biosens. Bioelectron.* **2015**, *69*, 167−173.
(36) Tonndorf, P.; Schmidt, R.; Bottger, P.; Zhang, X.; Borner, J.; Liebig, A.; Albrecht, M.; Kloc, C.; Gordan, O.; Zahn, D. R. T.; de Vasconcellos, S. M.; Bratschitsch, R. Photoluminescence Emission and Raman Response of Monolayer MoS_2, $MoSe_2$, and WSe_2. *Opt. Express* **2013**, *21*, 4908−4916.
(37) Eng, A. Y. S.; Ambrosi, A.; Sofer, Z.; Simek, P.; Pumera, M. Electrochemistry of Transition Metal Dichalcogenides: Strong Dependence on the Metal-to-Chalcogen Composition and Exfoliation Method. *ACS Nano* **2014**, *8*, 12185−12198.
(38) Ambrosi, A.; Sofer, Z.; Pumera, M. Lithium Intercalation Compound Dramatically Influences the Electrochemical Properties of Exfoliated MoS_2. *Small* **2015**, *11*, 605−612.
(39) Sekine, T.; Julien, C.; Samaras, I.; Jouanne, M.; Balkanski, M. Vibrational Modifications on Lithium Intercalation in MoS_2. *Mater. Sci. Eng., B* **1989**, *3*, 153−158.
(40) Terrones, H.; Del Corro, E.; Feng, S.; Poumirol, J. M.; Rhodes, D.; Smirnov, D.; Pradhan, N. R.; Lin, Z.; Nguyen, M. A. T.; Elias, A. L.; Mallouk, T. E.; Balicas, L.; Pimenta, M. A.; Terrones, M. New First Order Raman-Active Modes in Few Layered Transition Metal Dichalcogenides. *Sci. Rep.* **2015**, *4*, 4215.
(41) Sugai, S.; Ueda, T. High-Pressure Raman Spectroscopy in the Layered Materials 2H-MoS_2, 2H-$MoSe_2$, and 2H-$MoTe_2$. *Phys. Rev. B: Condens. Matter Mater. Phys.* **1982**, *26*, 6554−6558.
(42) Tongay, S.; Zhou, J.; Ataca, C.; Lo, K.; Matthews, T. S.; Li, J.; Grossman, J. C.; Wu, J. Thermally Driven Crossover from Indirect Toward Direct Bandgap in 2D Semiconductors: $MoSe_2$ *Versus* MoS_2. *Nano Lett.* **2012**, *12*, 5576−5580.
(43) Li, H.; Zhang, Q.; Yap, C. C. R.; Tay, B. K.; Edwin, T. H. T.; Olivier, A.; Baillargeat, D. From Bulk to Monolayer MoS_2: Evolution of Raman Scattering. *Adv. Funct. Mater.* **2012**, *22*, 1385−1390.
(44) Saito, R.; Tatsumi, Y.; Huang, S.; Ling, X.; Dresselhaus, M. S. Raman Spectroscopy of Transition Metal Dichalcogenides. *J. Phys.: Condens. Matter* **2016**, *28*, 353002.
(45) Berkdemir, A.; Gutierrez, H. R.; Botello-Mendez, A. R.; Perea-Lopez, N.; Elias, A. L.; Chia, C.−I.; Wang, B.; Crespi, V. H.; Lopez-Urias, F.; Charlier, J.-C.; Terrones, H.; Terrones, M. Identification of Individual and Few Layers of WS_2 Using Raman Spectroscopy. *Sci. Rep.* **2013**, *3*, 1755.
(46) Sahin, H.; Tongay, S.; Horzum, S.; Fan, W.; Zhou, J.; Li, J.; Wu, J.; Peeters, F. M. Anomalous Raman Spectrum and Thickness-Dependent Electronic Properties of WSe_2. *Phys. Rev. B: Condens. Matter Mater. Phys.* **2013**, *87*, 165409.
(47) Voiry, D.; Salehi, M.; Silva, R.; Fujita, T.; Chen, M.; Asefa, T.; Shenoy, V. B.; Eda, G.; Chhowalla, M. Conducting MoS_2 Nanosheets as Catalysts for Hydrogen Evolution Reaction. *Nano Lett.* **2013**, *13*, 6222−6227.
(48) Bai, S.; Wang, L.; Chen, X.; Du, J.; Xiong, Y. Chemically Exfoliated Metallic MoS_2 Nanosheets: A Promising Supporting Co-Catalyst for Enhancing the Photocatalytic Performance of TiO_2. *Nano Res.* **2015**, *8*, 175−183.
(49) Lukowski, M. A.; Daniel, A. S.; Meng, F.; Forticaux, A.; Li, L.; Jin, S. Enhanced Hydrogen Evolution Catalysis from Chemically Exfoliated Metallic MoS_2 Nanosheets. *J. Am. Chem. Soc.* **2013**, *135*, 10274−10277.
(50) Chang, K.; Hai, X.; Pang, H.; Zhang, H.; Shi, L.; Liu, G.; Liu, H.; Zhao, G.; Li, M.; Ye, J. Targeted Synthesis of 2H- and 1T-Phase MoS_2 Monolayer for Catalytic Hydrogen Evolution. *Adv. Mater.* **2016**, *28*, 10033−10041.
(51) Liu, G.; Lin, Y. Biosensor Based on Self-Assembling Acetylcholinesterase on Carbon Nanotubes for Flow Injection/Amperometric Detection of Organophosphate Pesticides and Nerve Agents. *Anal. Chem.* **2006**, *78*, 835−843.
(52) Cesarino, I.; Moraes, F. C.; Lanza, M. R. V.; Machado, S. A. S. Electrochemical Detection of Carbamate Pesticide in Fruit and Vegetable with a Biosensor Based on Acetylcholinesterase. *Food Chem.* **2012**, *135*, 873−879.
(53) Viswanathan, S.; Radecka, H.; Radecki, J. Electrochemical Biosensor for Pesticide Based on Acetylcholinesterase Immobilized on Polyaniline Deposited on Vertically Assembled Carbon Nanotubes Wrapped with ssDNA. *Biosens. Bioelectron.* **2009**, *24*, 2772−2777.

DOI: 10.1021/acsnano.7b01364
ACS Nano 2017, 11, 5774−5784

(54) Jha, N.; Ramaprabhu, S. Development of Au Nanoparticle Dispersed Carbon Nanotube-Based Biosensor for the Detection of Paraoxon. *Nanoscale* **2010**, *2*, 806−810.
(55) United States Department of Agriculture Agricultural Research Service: National Nutrient Database for Standard Reference Release 28. https://ndb.nal.usda.gov/ndb/search/list?qlookup=09003&format=Full (accessed 7 April 2017).
(56) Oliveira, A. C.; Mascaro, L. H. Evaluation of Acetylcholinesterase Biosensor Based on Carbon Nanotube Paste in the Determination of Chlorphenvinphos. *Int. J. Anal. Chem.* **2011**, *2011*, 974216.
(57) Bucur, M.-P.; Bucur, B.; Radu, G.-L. Critical Evaluation of Acetylthiocholine Iodide and Acetylthiocholine Chloride as Substrates for Amperometric Biosensors Based on Acetylcholinesterase. *Sensors* **2013**, *13*, 1603−1613.
(58) Taylor, P.; Radic, Z. The Cholinesterase: From Genes to Proteins. *Annu. Rev. Pharmacol. Toxicol.* **1994**, *34*, 281−320.
(59) Rosenberry, T. L. Acetylcholinesterase. *Adv. Enzymol. Relat. Areas Mol. Biol.* **2006**, *43*, 103−218.
(60) Riley, C. M.; Rosanske, T. M. *Development and Validation of Analytical Methods*; Elsevier: New York, 1996.
(61) Swartz, M. E.; Krull, I. S. *Analytical Method Development and Validation*; Marcel Dekker: New York, 1997.
(62) Ermer, J.; Miller, J. H. M. *Method Validation in Pharmaceutical Analysis*; Wiley VCH: Weinheim, 2005.
(63) De Bievre, P.; Gunzler, H. *Validation in Chemical Measurements*; Springer: Berlin, 2005.
(64) Ozkan, S. A. *Electroanalytical Methods in Pharmaceutical Analysis and Their Validation*; HNB Publishing: New York, 2012.
(65) Wang, L.; Dong, J.; Wang, Y.; Cheng, Q.; Yang, M.; Cai, J.; Liu, F. Novel Signal-Amplified Fenitrothion Electrochemical Assay, Based on Glassy Carbon Electrode Modified with Dispersed Graphene Oxide. *Sci. Rep.* **2016**, *6*, 23409.
(66) FAO Plant Production and Protection Paper No 178, Pesticide Residues in Food, 2004.
(67) Sale of Food Act, Cap 283 s 56(1), Food Regulations, Agri-Food and Veterinary Services, Singapore, 2005.

DOI: 10.1021/acsnano.7b01364
ACS Nano 2017, 11, 5774−5784